Millimeter Array Memo 21

Evaluation of Some Initial Possibilities for the Large Congurations of the Proposed mm Array

R. M. Hjellming

I. INTRODUCTION

This memo is the second in a series dealing with the simulation and evaluation of various proposals for a mm array operated as a national facility by NRAO. The first memo in the series (mm Array Memo 20) discussed some of the major parameters of the 1000, 300, 90, and 25 m. configurations of antennas that were called the 1km, 300m, 90m, and M-T configurations. This memo will mainly deal with an initial evaluation of the possibilities for the two larger arrays involving 15 <= N <= 27 antennas of diameter D = 9-13 m.

II. MAP AND BEAM SIZES

As discussed in mm array memo 20, the size of aperture synthesis maps is mainly determined by the ratio of the antenna beam size to the synthesized beam size. Table 1 shows the results obtained for large antennas with D = 10 m.

Table 1

Fields of View, Synthesized beams, and Map Sizes

Configuration	B	θ_{ant}	θ_{syn}	M	M_{na}	M_{FFT}
1km	1000 m	$22''\lambda_{mm}$	$0.19''\lambda_{mm}$	230	150	128-512
300m	300 m	$22''\lambda_{mm}$	$0.65''\lambda_{mm}$	70	45	64-128
90m	90 m	$22''\lambda_{mm}$	$2.2''\lambda_{mm}$	20	13	16-64

In Table 1 we have listed: (1) a sampling map size ($M = M_{un}$) for uniform weighting; (2) a sampling map size (M_{na}), for natural weighting analogous to that of the VLA; and (3) the "practical" map sizes that would typically be used because the FFT algorithm requires map sizes that are powers of two.

III. SOME POTENTIAL CONFIGURATIONS FOR THE LARGE mm ARRAY ANTENNAS

The most obvious configuration for a mm array with reasonably good characteristics for observing all parts of the sky, including southerly declinations near the Galactic Center, is a VLA-like configuration with N/3 antennas on each of three arms of a Y. However, there are other possibilities that can be considered for the larger configurations of the mm array, mainly because one need not be restricted by the limitations of a railroad-type antenna transportation system. In Figure 1 we show antennas locations for six different types of configurations that represent the main categories that will be discussed in the remainder of this memo: (a) a normal VLA-like "Y" with antennas located along each arm with radial distance proportional to the k = 1 to 9 antenna numbers raised to the 1.716 power; (b) a "Y" configuration with radial locations of antennas obeying a power law of $k^{0.9}$; (c) a "spiralized" "Y" in which the power law dependence of the VLA is retained, but each antenna location is rotated counterclockwise by an angle of $60(k/9)^{1.716}$ degrees; (d) a non-redundant 2-D array; (e) a circular array with four antennas at closer than average spacings to aid in filling in the center of the u-v plane; and (f) a circular array with antenna locations chosen by a random number generator.

The u-v plane coverage for the N = 27 case, taken from "An Introduction to the NRAO Very Large Array", is shown for a number of declinations in Figure 2. As has become standard practice with the VLA, the deficiencies of the Y-array at lower declinations can be considerable alleviated by making the northern arm of the Y a factor of three or so longer than the SE and SW arms. For the purposes of the present memo, we will assume that N-S elongation of each array will be part of the strategy for observing with the proposed mm array. For comparison with cases that we will discuss shortly, Figure 3 shows the u-v coverage and beam profiles (computed with both natural and uniform weighting) for a declination of 60 degrees and both one hour (at zenith) snapshots and 12 hours of tracking.

While a conservative approach would be to build VLA-like configurations of N antennas for the 1km and 300m configurations, there are a number of reasons for considering alternatives. Part of the reasoning behind the VLA Y-shape was the need to economize on the railroad track and stations that are an integral part of the VLA configuration and transportation system. However, for the mm array, with 9-13 m. antennas, one can use antenna transporters with rubber tires, allowing more flexibility in the location of stations. In addition, the location of antennas on linear arms causes dense accumulations of data points in the u-v plane for the three position angles, with respect to geocentric N-S, of 5, 125, and 245 degrees, which results in non-optimal u-v coverage for the snapshot observations which are a considerable fraction of VLA observations. This effect is shown in Figure 4 where both the u-v plane and a synthesized beam profile are shown for an instantaneous snapshot observation with N = 27 and a VLA-like antenna distribution.

One obvious way to retain most of the characteristics of the VLA-like Y configurations, while improving the u-v plane coverage and beam for snapshots, is to "spiralize" the Y by rotating the position angle of each antenna, with respect to the center, by an amount proportional to the radial distance from the center. Figure 5 shows the u-v coverage and beam for a snapshot observation with such a configuration, where the k-th antenna along each arm is rotated counter-clockwise by an angle $60*(k/9)^{1.716}$ degrees. It is obvious that the instantaneous u-v coverage and beams are somewhat improved. It is also possible that with tracking over a period of four hours or more, one will obtain roughly the same u-v plane coverage for a linear Y and a "spiralized" Y. In Figure 6 we show the u-v coverages and beam profiles for the spiralized Y for declinations of 60 degrees. A comparison of Figures 3 (Y27) and 6 show that there is little qualitative or quantitative difference between the 12 hour coverage beams; however, the naturally weighted snapshot beam has a distinctly narrower version of the broad plateau associated with naturally weighted beams.

As mentioned above, one can design many arrays with antennas located at radial distances proportional to k^p, where k is an antenna number for radial rings (p = 1.716 for the VLA-like case). A power law in radial location from the center of the array leads to the same order of power law for the density of measured data points in radial rings in the u-v plane. For the VLA case the local density of points in the inner part of the u-v plane is roughly two orders of magnitude greater than the local density in the outer parts of the sampled u-v plane. One can conceive of other power laws that alter the relative sampling of different fourier components, and one of the primary conclusions of this memo will be the obvious - VLA-like power laws improve the sensitivity to extended surface brightness features. In Figure 7 we see the u-v coverages and beam profiles for the array in Fig. 1b, which has a radial power law with a power of 0.9. Comparing Figures 3 (Y27) and 7, the beams for Y27R0.9 have distinctly larger far sidelobes that one has with Y27, however the natural weight 12 hour coverage beam for Y26R0.9 has a narrower base.

Another configuration that is often discussed is the "classical" configuration of antennas arranged on a circle (or ellipses elongated in the N-S direction for low declination observations). Figure 8 shows the u-v coverages and beam profiles for both snapshot and full coverage observations with this configuration (for a declinatilon of 60 degrees). One of the undesirable characteristics of the circular array is the large hole in the center of the u-v plane. One obvious improvement is to add a few antennas at locations on the circle, but between the normal spacings. An example of 24 antennas at even spacings on the circle, and three antennas on a spur located near one antenna (cf. Fig. 1e) was used to generate the plots shown in Figure 9. Another of the undesireable characteristics of the circular array is the sidelobe ringing and high redundancy implicit in even separations. Avoiding equal interval spacings along the circle will reduce both of these undesireable effects; therefore we used a program to generate random locations around a circle, subject to a constraint that antennas could not be too close to each other. Fig. 1f shows one of the best of these configurations, and Figure 10 shows the u-v plane coverage and beam profiles for this configuration. If beam sidelobes are the primary criteria, a circular array, and R2Cir27 in particular, is better than any of the arrays discussed so far. This conclusion is supported by both the quantitative evaluations of beam sidelobe level, based on the equations derived in mm array memos 18 and 20, and the qualitative impressions from the u-v planes and beams in Figures 3 and 6-10.

In Figure 1d we show an example of a non-redundant array of antennas in two dimensions that was obtained from T. Cornwell. The u-v coverage and beam profiles for snapshot and full track observations at declinations of 60 degrees are shown in Figure 11 for this array. Both qualitative and quantitative aspects favor R2Cir27 over NonRed27 by a small margin. However, this was a very early attempt to obtain a "randomized" 2-D array, hence it is quite possible that other arrays based upon the same principle would be even better.

Although many of the Figures just discussed have numerical indications of sidelobe level, let us now discuss these quantitative evaluations in more detail, particularly since the indications from surface brightness criteria will end up giving recommendations that are different from those derived from only the u-v plane and sidelobe considerations discussed so far.

IV. SIDELOBES AND SURFACE BRIGHTNESS SENSITIVITY

The ultimate criteria for sidelobe level and surface brightness signal/noise is the desired occupancy of the cells in the gridded u-v plane. As discussed by T. Cornwell in mm array memo 18, the rms sidelobe level for a naturally weighted beam, σ_{na}, is given by

$$\sigma^2_{na} = \sum_{j=1}^{M} \sum_{k=1}^{M} (T(u,v)*N_{jk})^2/(\sum_{j=1}^{M} \sum_{k=1}^{M} T(u,v)*N_{jk})^2 \qquad (1)$$

where N_{jk} is the number of u-v data points within the i-j cell of an M X M grid, and T(u,v) is a taper function for the u-v plane. For uniform weighting

$$\sigma^2_{un} = \sum_{j=1}^{M} \sum_{k=1}^{M} (T(u,v)*\delta_{jk})^2/(\sum_{j=1}^{M} \sum_{k=1}^{M} T(u,v)\delta_{jk})^2 \qquad (2)$$

$$= 1/N_{eff.occupied}$$

where δ_{jk} = 1 if any data points are within the cell, and = 0 otherwise. Thus $N_{eff.occupied}$ is the effective number of occupied cells, which will be equal to the actual number of occupied cells only when T(u,v) = 1.

The taper function that we will use is that of a Gaussian of the form

$$T(u,v) = \exp[-0.25f(u^2 + v^2)/r^2_{max}] \qquad (3)$$

where r_{max} is the maximum antenna separation and f is a taper parameter allowing one to specify the fractions of r_{max} that will effectively be included in the u-v plane.

Now we need to remind ourselves of the criteria for surface brightness sensitivity. This was discussed initially by T. Cornwell in mm Array Memo 18, and was summarized in mm Array Memo 20. In order to relate brightness temperature to the noise level of inidividual data points, let us take

$$\sigma_v = (0.78/D_m)(T_{sys}/100)(1\mathrm{GHz}/\Delta\nu)^{1/2} \quad \mathrm{Jy} \tag{4}$$

(cf. Eqn. 2-48 in "An Introduction to the NRAO VLA") which is the rms noise fluctuation for a single pair of antennas of diameter D_m, aperture efficiency of 0.5, bandwidth of 1 GHz, and a system temperature of 100 K. The surface brightness sensitivity formula given by mm Array Memos 18 and 20 is

$$T_b = 377 \; r_{km}^2 \; \sigma_v / [\sum_{j=1}^{M} \sum_{k=1}^{M} N_{jk} T_{jk}^2]^{1/2} \quad {}^{o}\mathrm{Kelvin} \tag{5}$$

where we have used the expression for the half-power beam width of a u-v plane r_{km} (km units) in radius, corresponding either to the actual maximum baseline or the effective radius after tapering with Equation (3). We will be evaluating surface brightness sensitivity in terms of T_b as a function of r.

V. THE RADIAL DISTRIBUTION OF u-v POINTS

One of the principal factors effecting the difference between the sidelobe levels with uniform and natural weighting is the radial distribution of data points in the u-v plane. Illustrating this we show in Figure 12 the beam profiles for a 300 m. VLA-like "Y" of 27 antennas obtained with both natural and uniform weighting. The enormous difference between the beams in Figure 12 is due to the $r^{1.716}$ distribution of antennas along each arm of a VLA-like Y; this results in a similar radial density of points in the u-v plane. In Figure 13 we show the plot of the population in annular rings in the u-v plane for four configurations that are variations on a VLA-like "Y": (a) the Y27 configuration with a 1.716 power law; (b) a "spiralized" version (Y27R60) of Y27 (cf. Fig 1c); (c) a "Y" configuration with a 0.9 power law; and (d) a "Y" configuration with a 0.5 power law. One can see from Figures 13a and 13b that N(u,v;r), once one gets away from the effect of the central "hole", is roughly proportional to $r_{uv}^{-1} = (u^2+v^2)^{-1/2}$ for both the VLA-like Y27 and the spiralized Y26R60. The power laws of 0.9 and 0.5, in an otherwise normal "Y", increase the proportion of points in the outer parts of the u-v plane as seen in Figures 13c and 13d, respectively. The bimodal characteristics of Fig. 13d are a result of having short spacings only when the antennas at the ends of arms correlated with each other, and there are not enough intermediate spacings due to cross-correlation of closely spaced antennas on different arms.

The characteristics of the u-v plane population for various circular, and a non-redundant 2-D array (Fig. 1d), are shown in Figure 14. The non-redundant array has a relatively flat distribution as seen in Fig. 14a. Figures 14b-14d indicate that all the circular arrays have distribuitions proportional to r_{uv}.

Since the area in each equal thickness ring in Fig. 13-14 is proportional to r_{uv}, that means the local density in the u-v plane is nearly proportional to r_{uv}^{-2} for the VLA-like Y (probably more like $r_{uv}^{-1.72}$); however, the circular arrays have, to first order, a uniform local density of points in the u-v plane.

Because the mm array will be very heavily used for mapping of extended surface brightness "objects", one of the major questions is: what is the relative utility of arrays with local densities in the u-v plane that are proportional to r_{uv}^{-2} (VLA-like), r_{uv}^{-1} (like the non-redundant 2-D arrays), or are roughly constant (e.g. circular arrays). Before commenting further on this issue, let us finally get to the section where we summarize quantitative results for these and other arrays.

VI. RESULTS FOR SIDELOBE LEVELS AND SURFACE BRIGHTNESS SENSITIVITIES

In Table 2 we present the results for the sidelobe levels for some of the arrays discussed above. The normal VLA-like Y for N antennas is designated by YN; the "spiralized" Y with a maximum rotation angle of 60 degrees is designated YNR60; two "Y"-arrays with radial power laws of $r^{0.9}$ and $r^{0.5}$ are designated by Y27R0.9 and Y27R0.5, respectively; a two-dimensional non-redundant array of 27 antennas supplied by T. Cornwell is designated by Non Red27; a 27 antenna configuration on a circle with even spacings around the circumference is denoted Cir27; a circular array of antennas, with 24 spaced evenly around the circumference and a spur of three antennas located between two normal spacing on the north (or south) side of the array, is designated Cir27Mod; and, finally, three circular arrays obtained by using a random number generator to select locations, subject to the constraint that arrays with physically overlapping antennas are rejected, are designated R1Cir27, R2Cir27, and R3Cir27.

Common parameters for the simulations in Table 2 were: frequency of 100 GHz; scan length of 1 hour or 12 hours; maximum antenna separation of 300 m. and u-v plane gridded with a size of 1000 nanoseconds; antenna diameter of 10 m.; a bandwidth of 1 GHz; and a sample time of 5 minutes. The brightness temperature (T_b) limits in Table 2 are for zero taper (f=0).

On the basis of these numbers, and ignoring any other considerations except avoidance of major sidelobe "ringing", one would choose one of the circular arrays, probably R2Cir27. However, this array is not the best for extended surface brightness measurements. In Figure 15 we plot the (rms) surface brightness sensitivity, Tb(mK) (units of milliKelvin), as a function of r_{km} (in units of kilometers) calculated from Equation (5). The left ordinate axis in Figure 15 applies to the full 1 GHz bandwidth, while the right ordinate axis applies to a bandwith of 100 kHz. The latter is the smallest spectral line channel width that is normal used for spectral line observing, giving velocity resolution of 0.26 km/sec.

The sensitivity of Y27 to fourier components above two beam-widths in size is significantly better than that for NonRed27 and R2Cir27, and slightly better than, Y27R0.9. The curves obtained for the four 300m configurations in Figure 15 should, in principle, scale with r^2_{max}, therefore we have plotted dashed curves in Figure 15 indicating the Y27 array scaled to the 1km and 90m configurations. All of the abovementioned results are for natural weighting. The uniform weighting results for all four configurations are indistinguishable and are plotted as the dotted curve in Figure 15. Finally, the lower envelope for these results for the Y27 array can be expressed by the following equation, which is basically valid for all tapers down to a factor of three less than r_{max},

$$T_b = 7.5\ r^2_{km}\ (T_{sys}/100)/[(D_m/10)[(\Delta\nu/1\mathrm{GHz})(\Delta t_{hrs}/12)N(N-1)/702]^{1/2}]\ \mathrm{mK} \quad (6)$$

The different slopes, between 50 and 30 km, for the four 300 m configurations plotted in Figure 15 directly reflect their power law distributions in the u-v plane, as discussed above.

Since much of the variation in T_b in Figure 15 is due to the r^2_{km} term, it is useful to remove this effect, which is due solely to the beam size and has nothing to do with u-v plane distributions. In Figure 16 we plot T_b/r^2_{km}, for both 1 GHz and 100 kHz bandwidths, as a function of r_{km} and r/r_{max}. The different brightness temperature sensitivities for the four arrays is more obvious in Figure 16. The plots of T_b/r_{km}^2 vs r/r_{max} are, in fact, valid for all size scales of each type of configuration, since only the relative distribution of points in the u-v plane will affect surface brightness sensitivity.

VII. THE PROBLEM OF THE COMPACT 90 METER CONFIGURATION

It is not possible to arrange 15-27 antennas in VLA-like "Y", 90 meters in diameter without serious shadowing and other problems. We must therefore consider other possibilities. Rather than include a discussion of this in the present memo, we defer the discussion of the 90m array to the memo on the M-T array, because similar options for packing will be considered.

VIII. CONCLUSIONS

The "best" arrays discussed in this memo, in terms of sidelobe characteristics, are the arrays R2Cir27 and and NonRed27. However, it is clear that the $r^{1.716}$ power law of the VLA-like Y27 is what gives it the best, by almost a factor of two, sensitivity to extended surface brightness features. It is obvious that the radial distribution of the circular array cannot be altered, however one can impose an r^2 radial distribution upon antenna locations that are otherwise random in x- and y-coordinates. If this is possible, then it may become the most superior array, by both sidelobe and surface brightness criteria. Failing this, the VLA-like Y27 configuration is probably best for the 1km and 300m mm arrays whose primary objectives are extended regions of emission.

Table 2

Parameters Obtained for Various 300 m. mm Arrays and 60 Degree Declination

	Horizon to Horizon Track (HA = -6^h to 6^h)				Snapshot (HA = -0.5^h to 0.5^h)			
Config.	σ_{na}	σ_{un}	Tb(mK)		σ_{na}	σ_{un}	Tb(mK)	
Y27	0.0510	0.0253	0.678	3.86	0.0596	0.0355	2.35	5.42
Y24	.0494	.0256	.765	3.90	.0610	.0378	2.65	5.77
Y21	.0482	.0260	0.877	3.97	.0610	.0415	3.04	6.22
Y18	.0466	.0265	1.027	4.05	.0629	.0454	3.56	6.90
Y15	.0450	.0272	1.240	4.14	.0641	.0510	4.29	7.77
Y27R60	.0481	.0255	0.678	3.88	.0545	.0367	2.35	5.59
Y21R60	.0454	.0263	.877	4.01	.0548	.0420	3.04	6.41
Y27R0.9	.0427	.0251	.678	3.83	.0621	.0346	2.35	5.28
Y27R0.5	.0398	.0245	.678	3.73	.0546	.0347	2.35	5.28
NonRed27	.0316	.0244	.678	3.72	.0386	.0309	2.35	4.72
Cir27	.0334	.0240	.678	3.65	.0403	.0317	2.35	4.83
Cir27Mod	.0321	.0240	.678	3.65	.0397	.0312	2.35	4.76
R1Cir27	.0296	.0239	.678	3.64	.0402	.0307	2.35	4.68
R2Cir27	.0282	.0239	.678	3.65	.0351	.0287	2.35	4.39
R3Cir27	0.0313	0.0240	.678	3.65	0.0438	0.0319	2.35	4.86

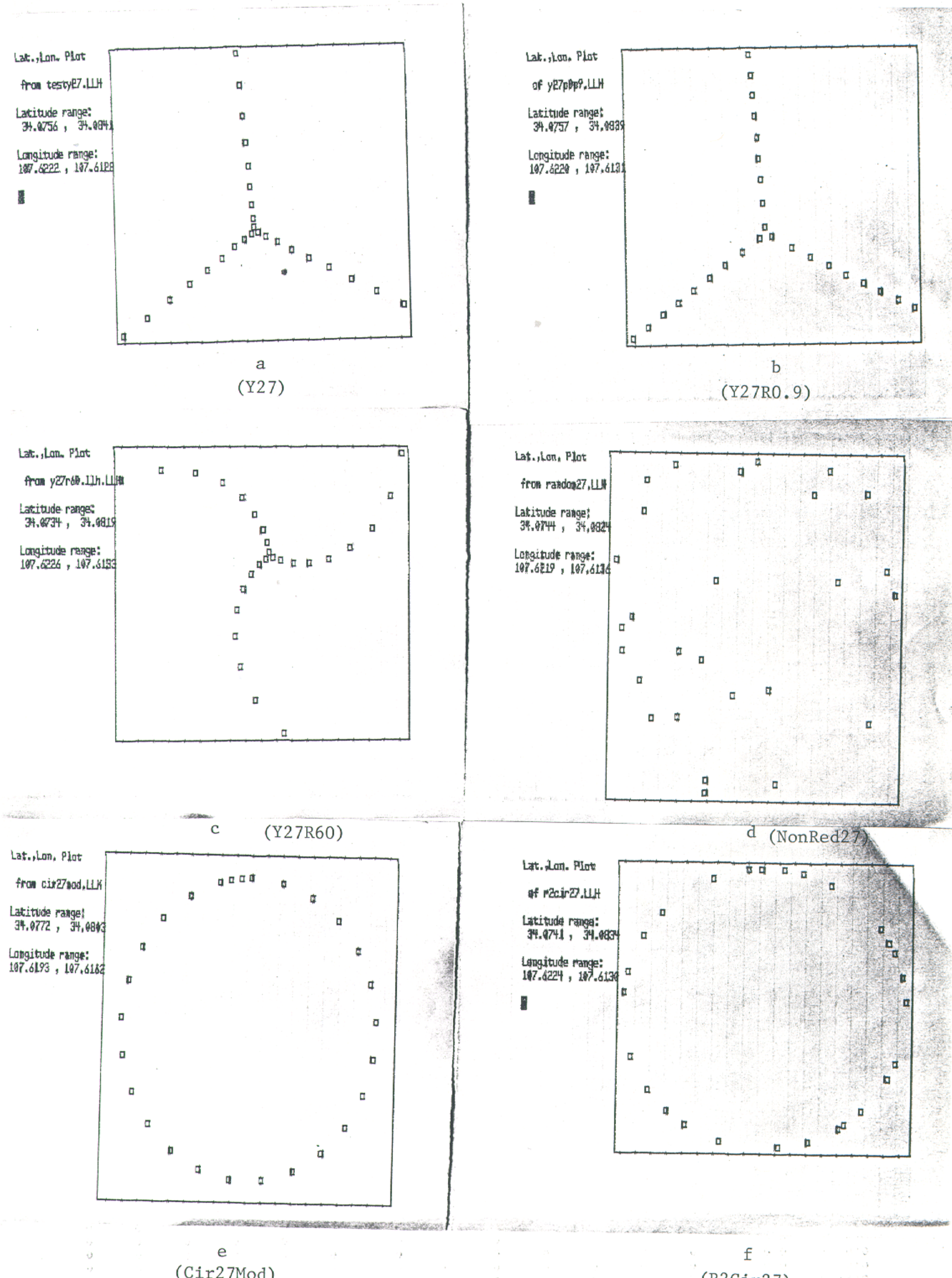
Lat.,Lon. Plot
from testy27.LLH
Latitude range:
34.0756 , 34.0841
Longitude range:
107.6222 , 107.6128
a
(Y27)
Lat.,Lon. Plot
of y27p0p9.LLH
Latitude range:
34.0757 , 34.0839
Longitude range:
107.6220 , 107.6131
b
(Y27R0.9)
Lat.,Lon. Plot
from y27r60.llh.LLH
Latitude range:
34.0734 , 34.0819
Longitude range:
107.6226 , 107.6153
c (Y27R60)
Lat.,Lon. Plot
from random27.LLH
Latitude range:
34.0744 , 34.0824
Longitude range:
107.6219 , 107.6136
d (NonRed27)
Lat.,Lon. Plot
from cir27mod.LLH
Latitude range:
34.0772 , 34.0843
Longitude range:
107.6193 , 107.6162
e
(Cir27Mod)
Lat.,Lon. Plot
of r2cir27.LLH
Latitude range:
34.0741 , 34.0834
Longitude range:
107.6224 , 107.6130
f
(R2Cir27)

Figure 1

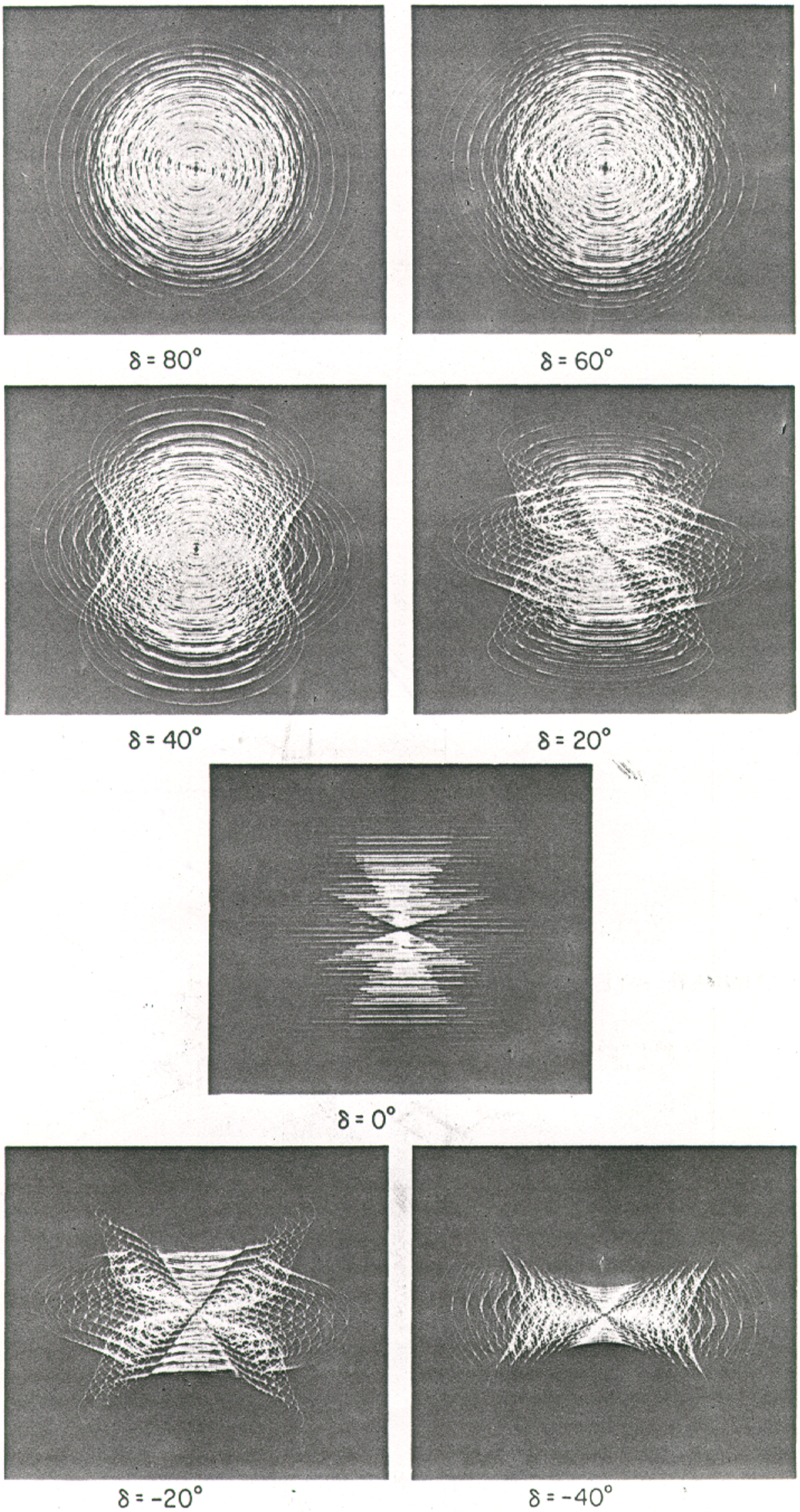

Figure 2-12. Possible u-v plane coverage with the 27-antenna VLA for declinations of 80°, 60°, 40°, 20°, 0°, -20°, and -40°.

Figure 2

(Y27)

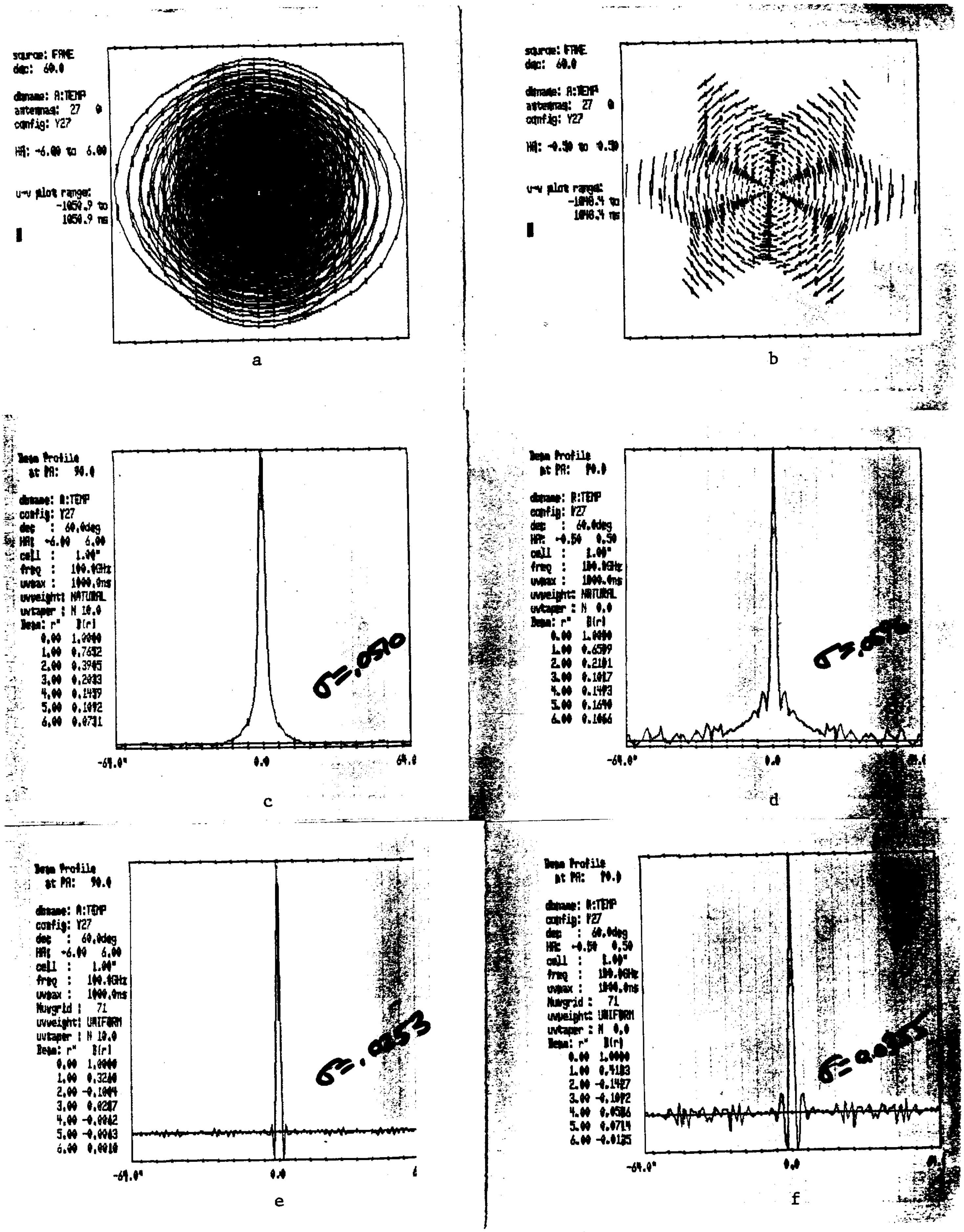

source: FAKE
dec: 60.0
dbname: A:TEMP
antennas: 27 0
config: Y27
HA: -6.00 to 6.00
u-v plot range:
-1050.9 to
1050.9 ns
a
source: FAKE
dec: 60.0
dbname: A:TEMP
antennas: 27 0
config: Y27
HA: -0.50 to 0.50
u-v plot range:
-1048.4 to
1048.4 ns
b
Beam Profile
at PA: 90.0
dbname: A:TEMP
config: Y27
dec : 60.0deg
HA: -6.00 6.00
cell : 1.00"
freq : 100.0GHz
uvmax : 1000.0ns
uvweight: NATURAL
uvtaper : N 10.0
Beam: r" B(r)
0.00 1.0000
1.00 0.7632
2.00 0.3945
3.00 0.2033
4.00 0.1439
5.00 0.1092
6.00 0.0731
σ=.0510
-64.0" 0.0 64.0
c
Beam Profile
at PA: 90.0
dbname: A:TEMP
config: Y27
dec : 60.0deg
HA: -0.50 0.50
cell : 1.00"
freq : 100.0GHz
uvmax : 1000.0ns
uvweight: NATURAL
uvtaper : N 0.0
Beam: r" B(r)
0.00 1.0000
1.00 0.6509
2.00 0.2101
3.00 0.1017
4.00 0.1493
5.00 0.1690
6.00 0.1066
-64.0" 0.0
d
Beam Profile
at PA: 90.0
dbname: A:TEMP
config: Y27
dec : 60.0deg
HA: -6.00 6.00
cell : 1.00"
freq : 100.0GHz
uvmax : 1000.0ns
Nuvgrid : 71
uvweight: UNIFORM
uvtaper : N 10.0
Beam: r" B(r)
0.00 1.0000
1.00 0.3240
2.00 -0.1004
3.00 0.0217
4.00 -0.0042
5.00 -0.0043
6.00 0.0010
σ=.0253
-64.0" 0.0
e
Beam Profile
at PA: 90.0
dbname: A:TEMP
config: Y27
dec : 60.0deg
HA: -0.50 0.50
cell : 1.00"
freq : 100.0GHz
uvmax : 1000.0ns
Nuvgrid : 71
uvweight: UNIFORM
uvtaper : N 0.0
Beam: r" B(r)
0.00 1.0000
1.00 0.4183
2.00 -0.1427
3.00 -0.1092
4.00 0.0586
5.00 0.0714
6.00 -0.0135
-64.0" 0.0
f

Figure 3
(Y27)

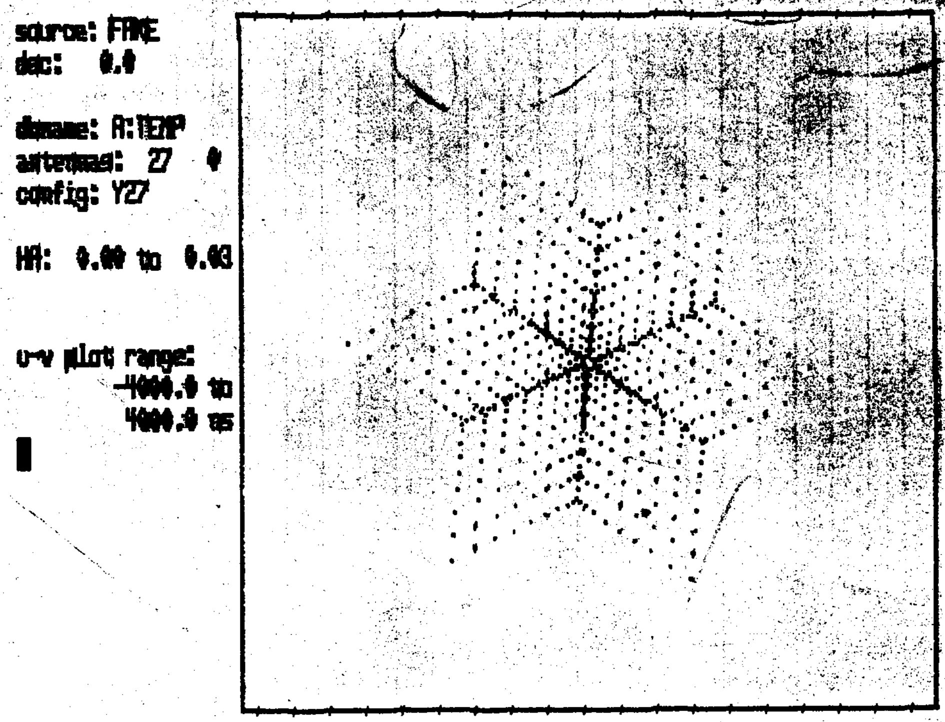

a

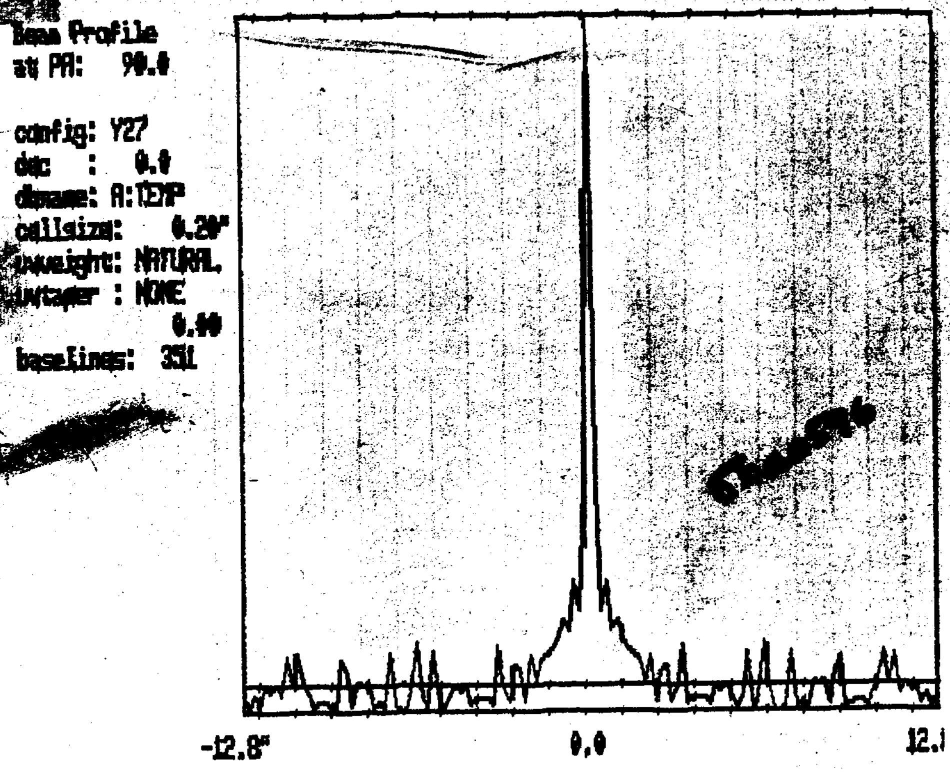

b.

Figure 4

(Y27)

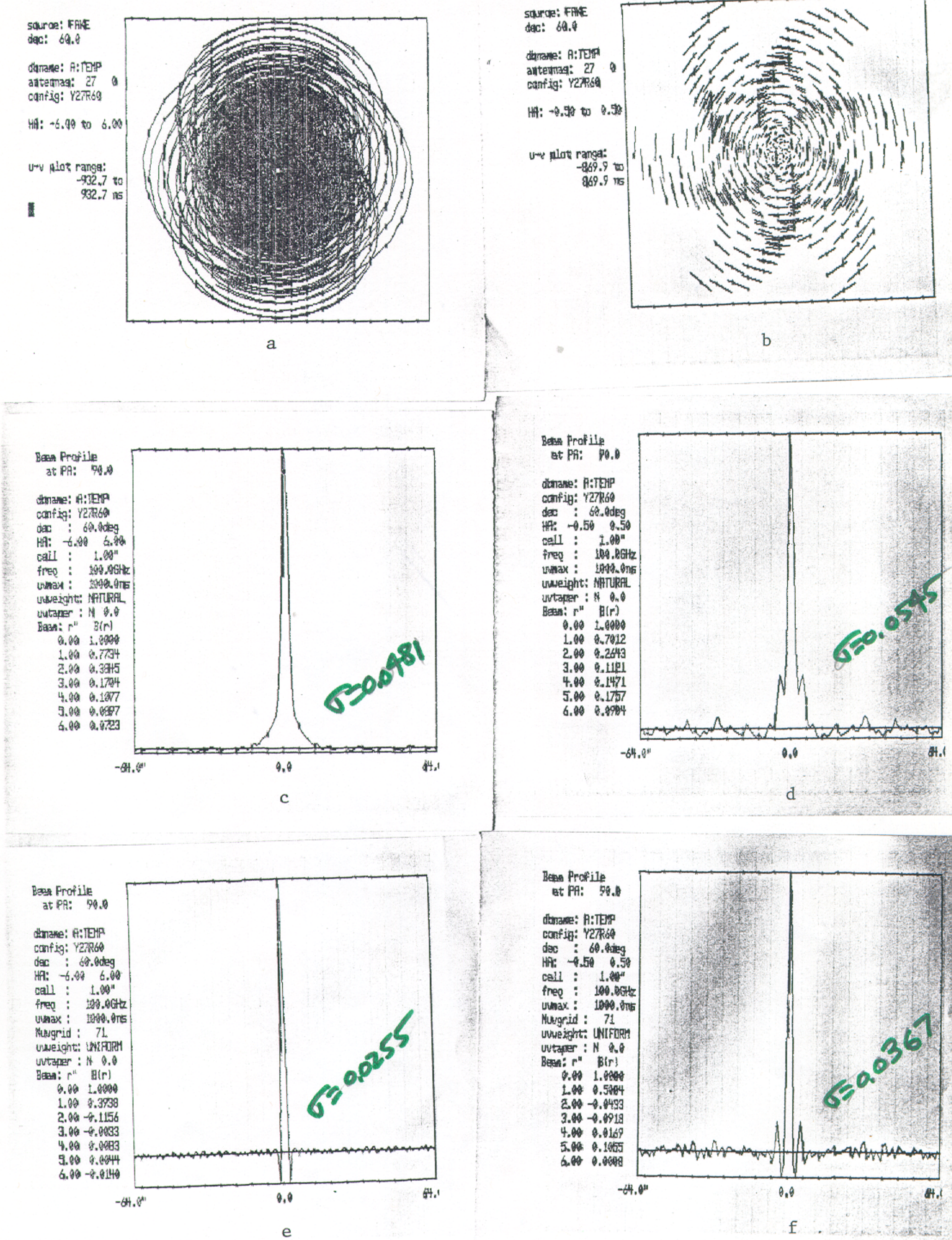

Figure 6

(Y27R60)

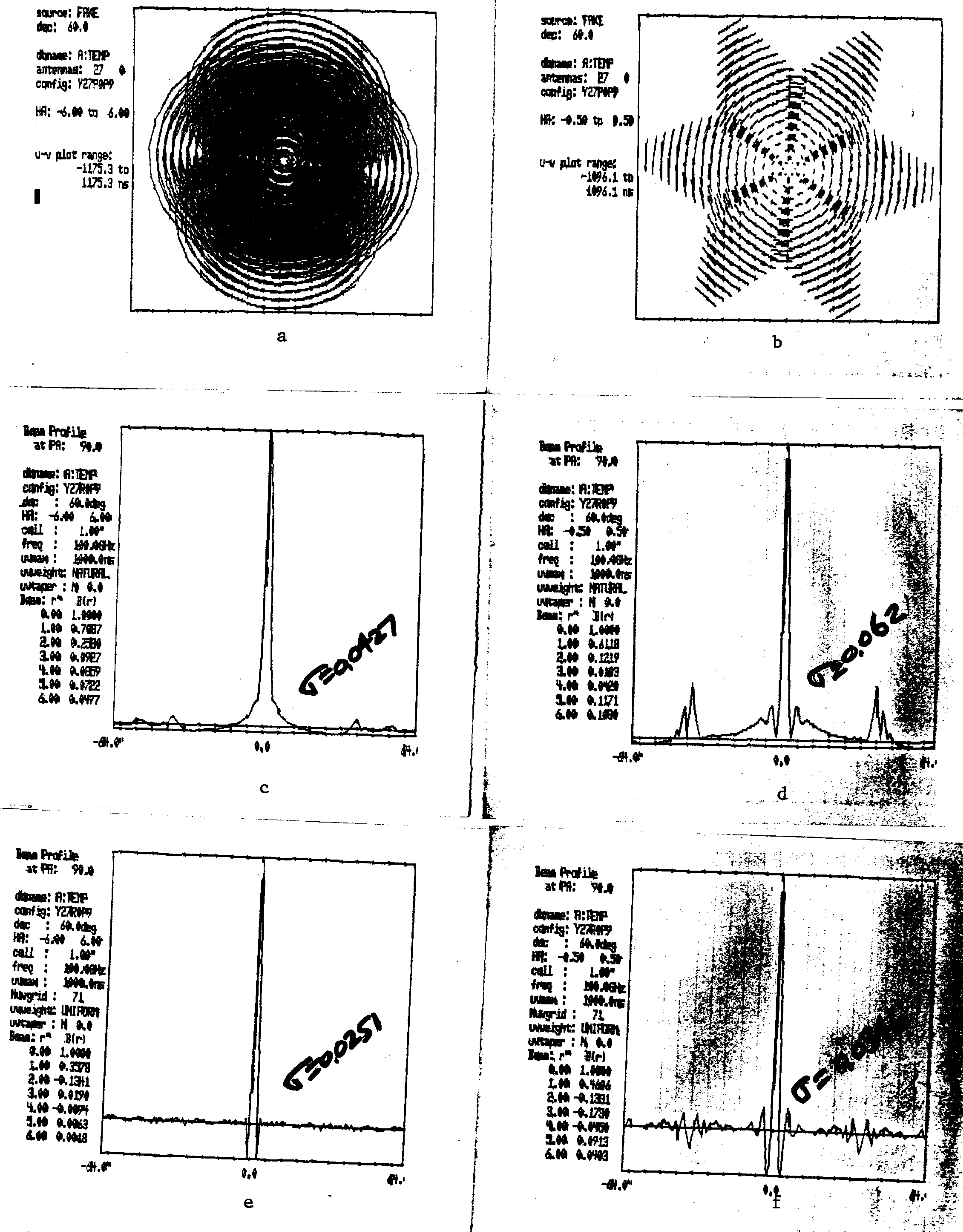

Figure 7

(Y27P0.9)

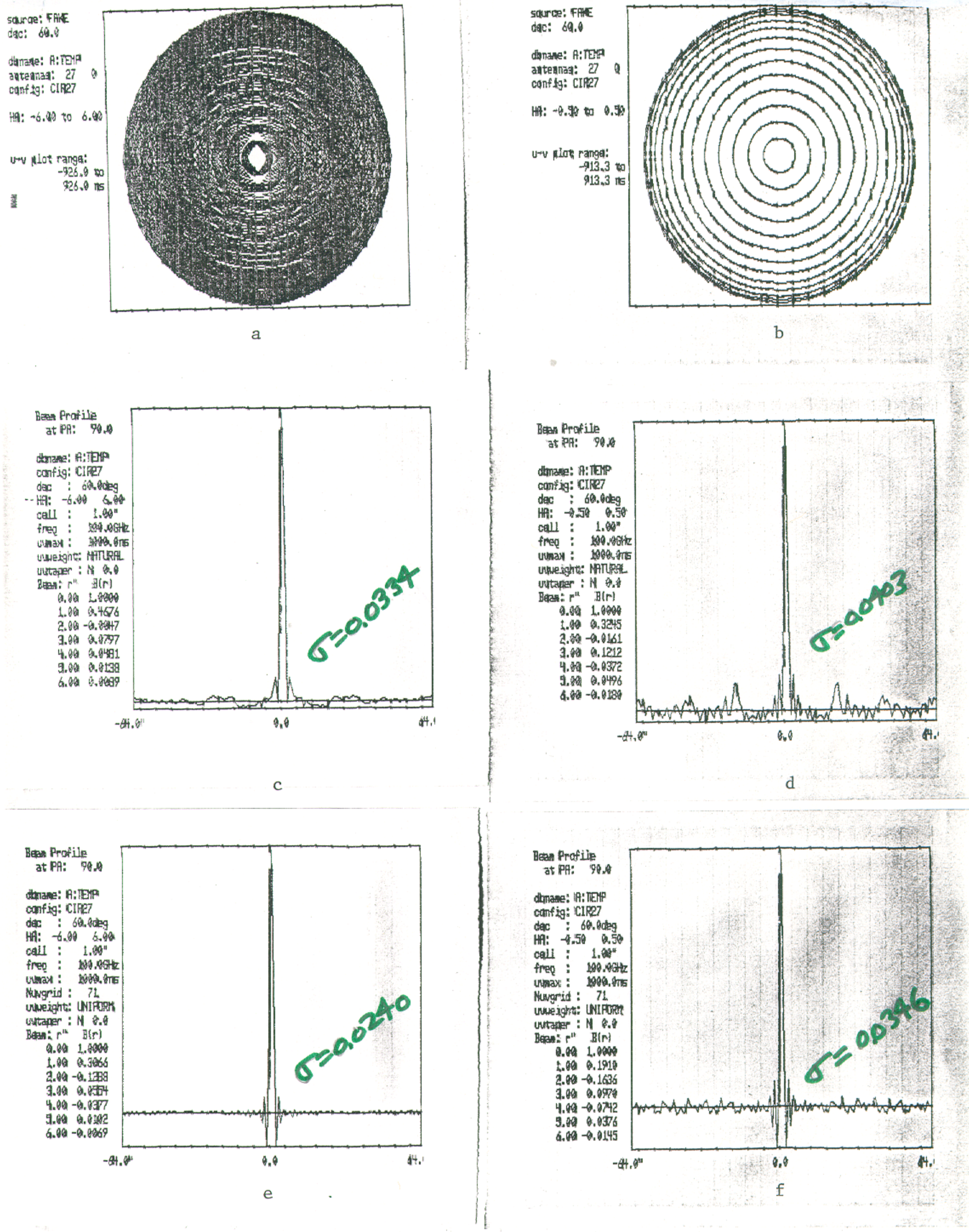

Figure 8

(Cir27)

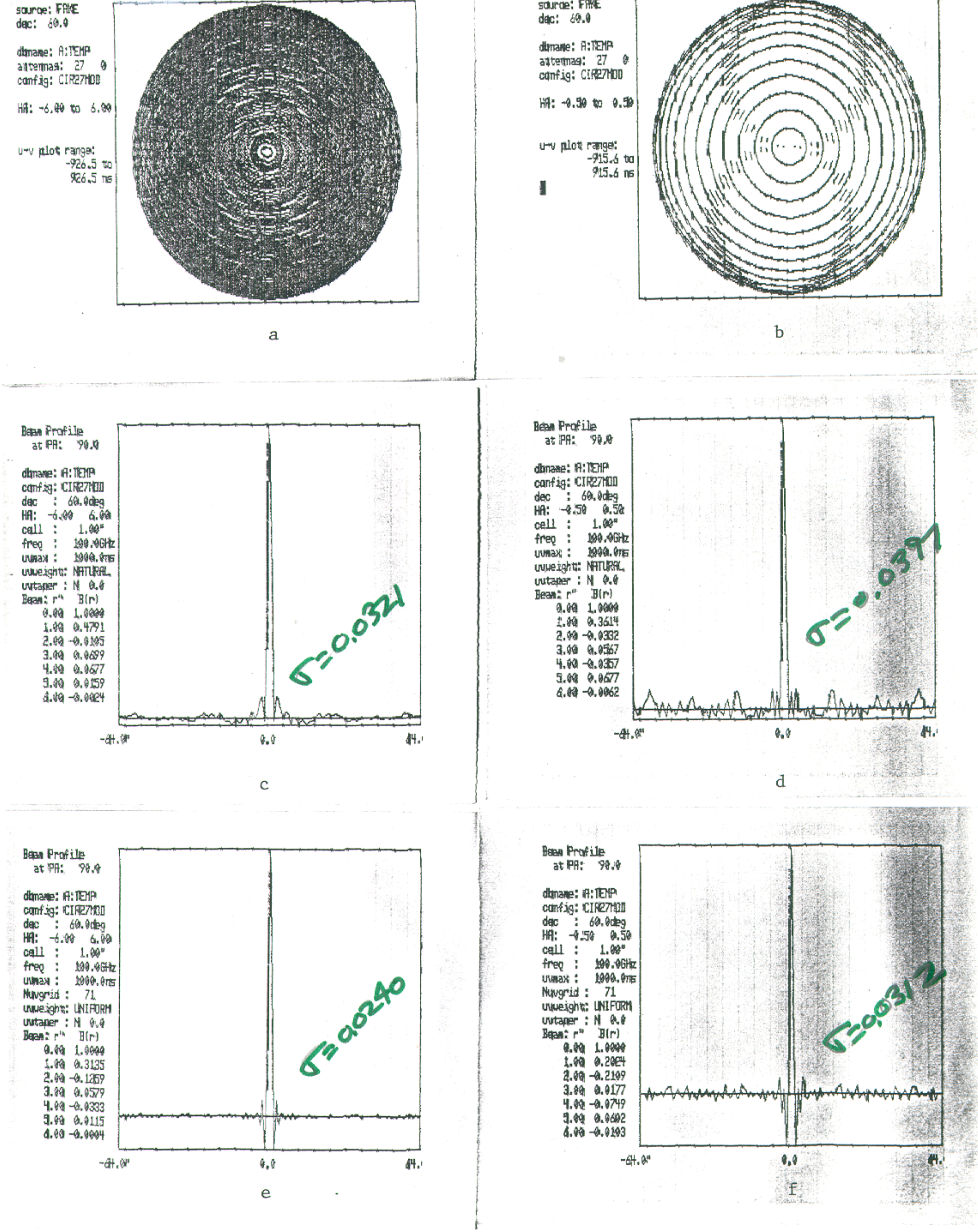

Figure 9

(Cir27Mod)

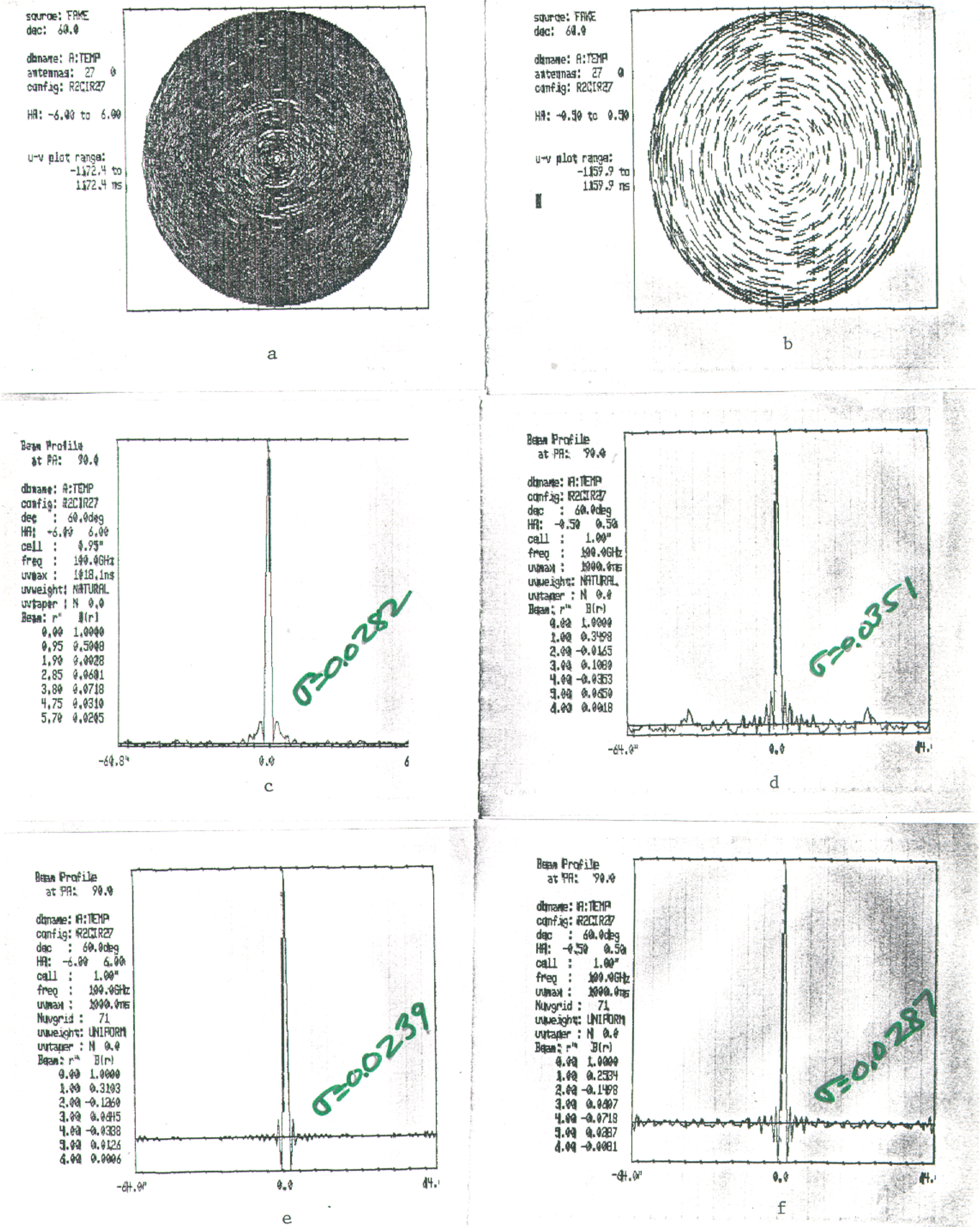

Figure 10

(R2Cir27)

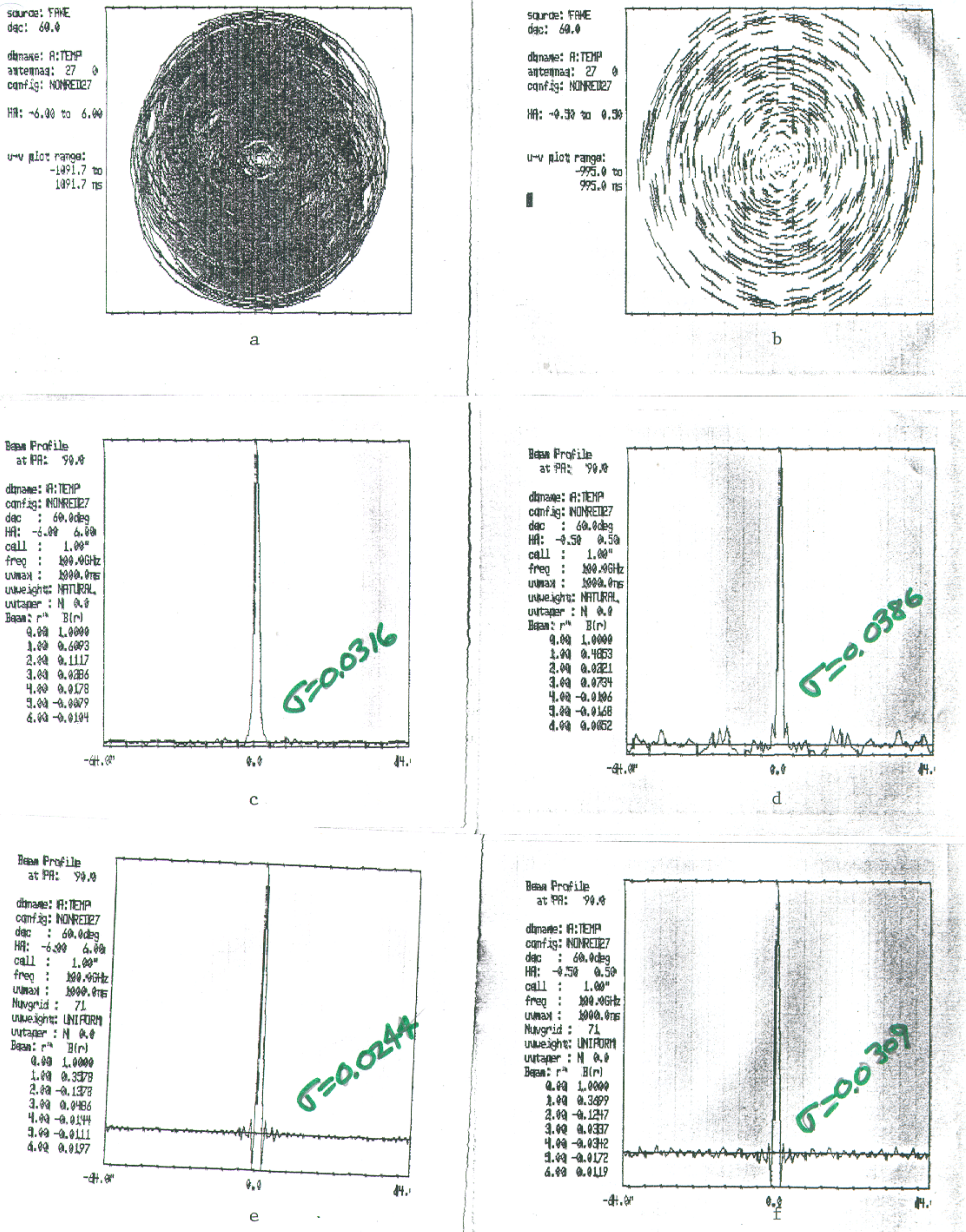

Figure 11

(NonRed27)

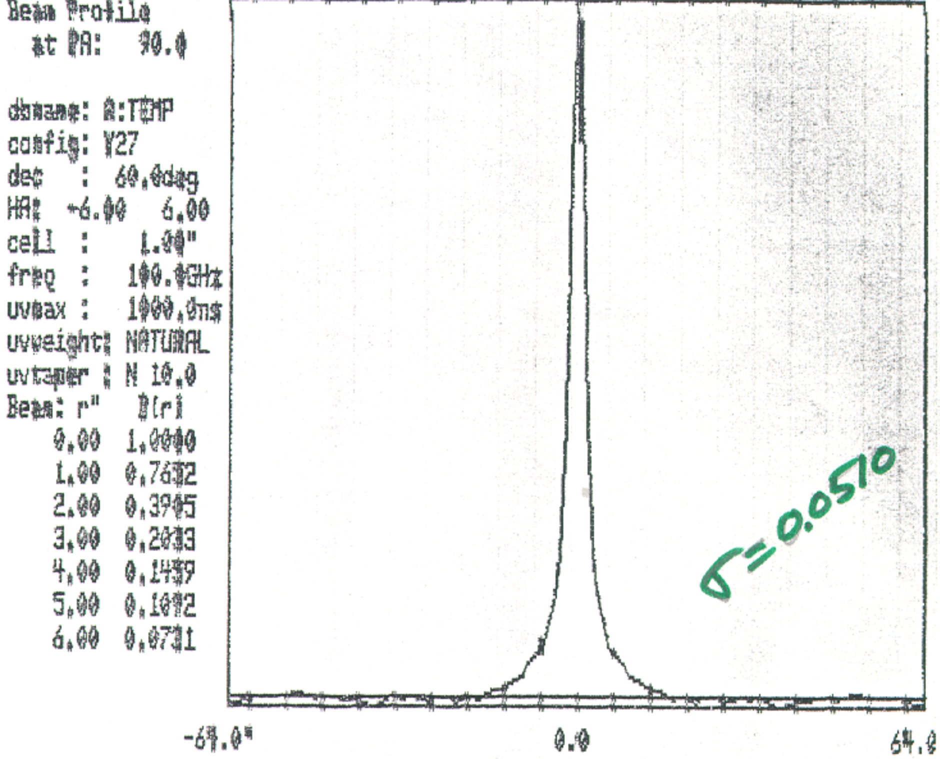

a

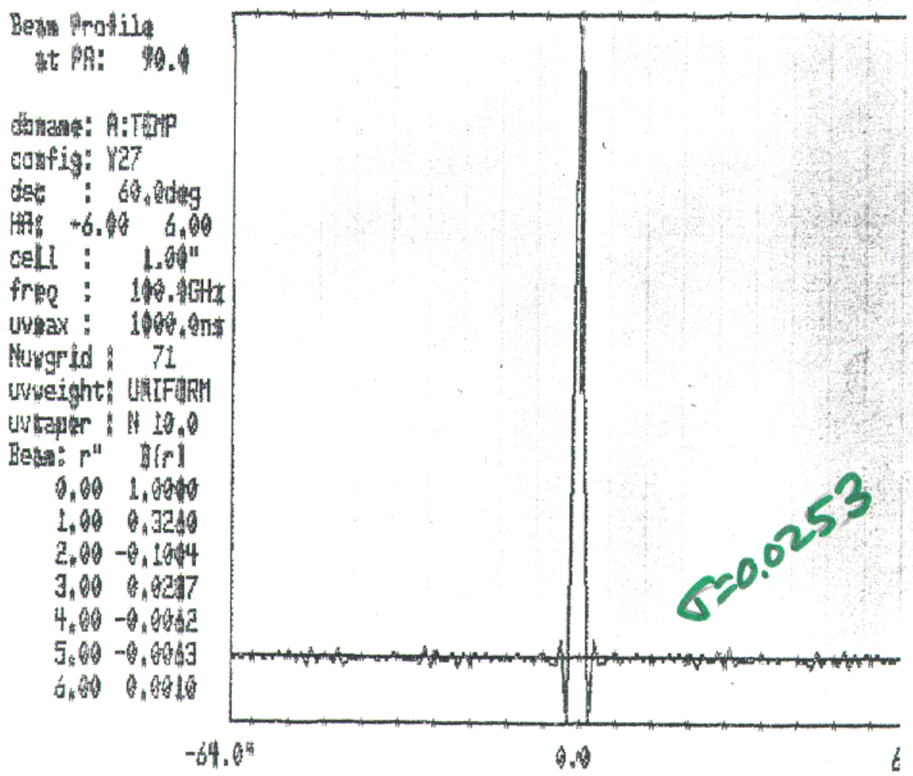

b

Figure 12

(Y27)

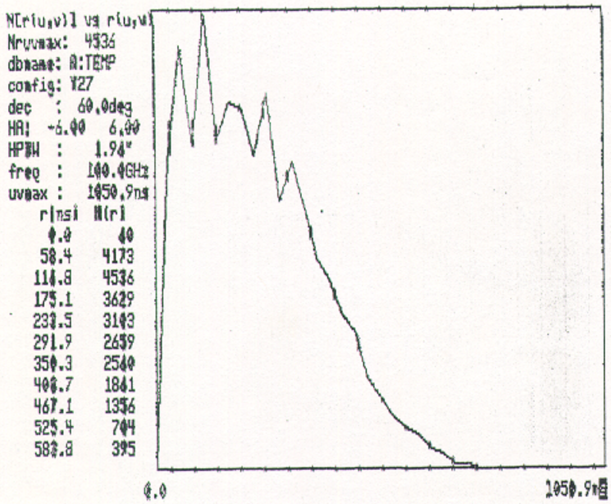

a
(Y27)

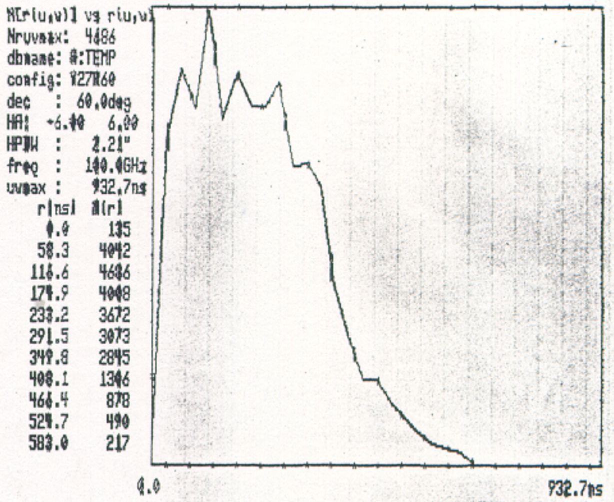

b
(Y27R60)

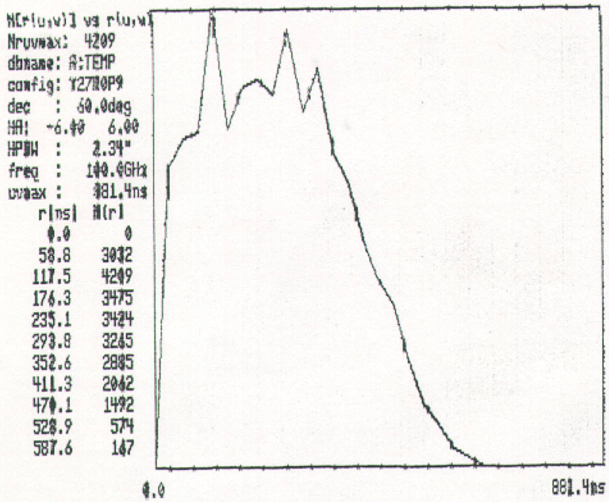

c
(Y27R0.9)

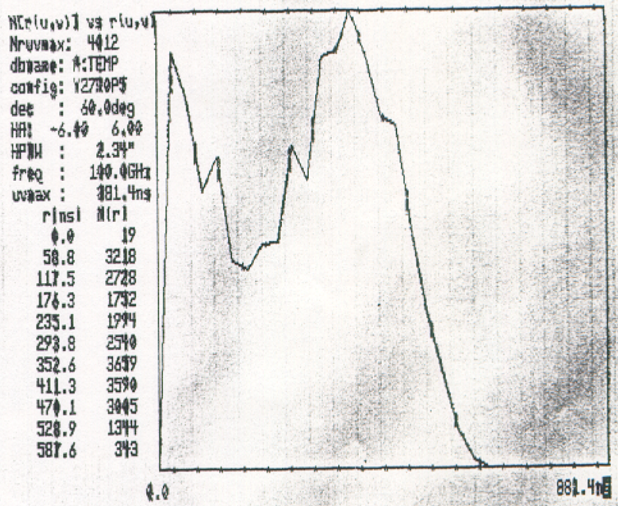

d
(Y27R0.5)

Figure 13

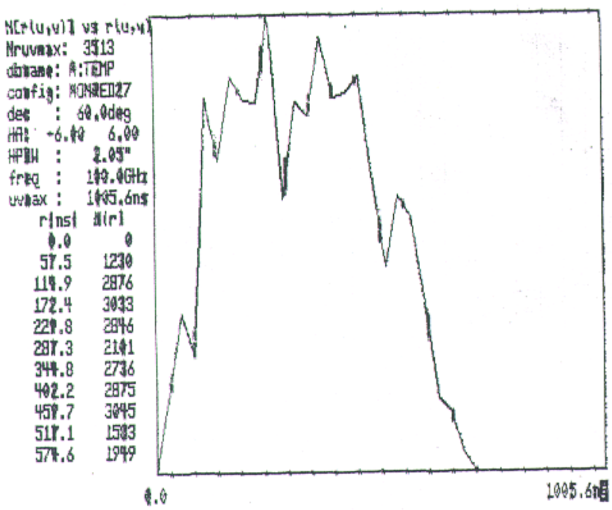

a
(NonRed27)

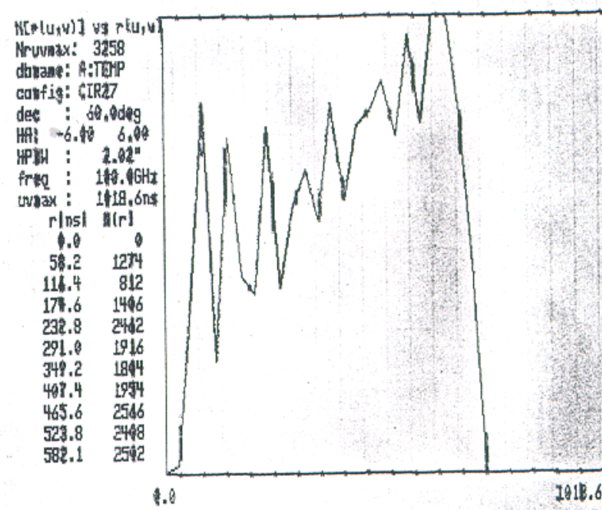

b
(Cir27)

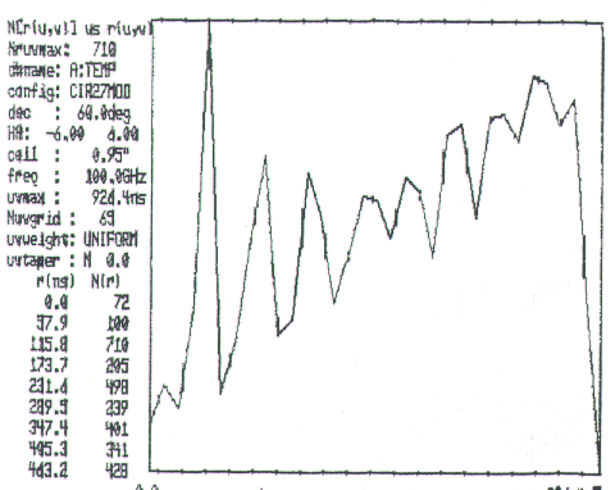

c
(Cir27Mod)

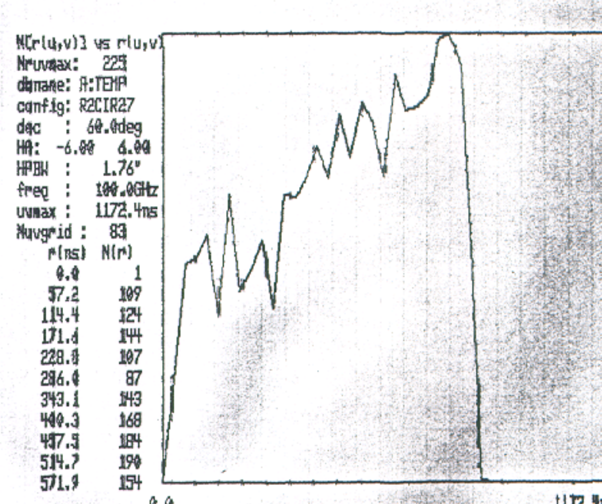

d
(R2Cir27)

Figure 14

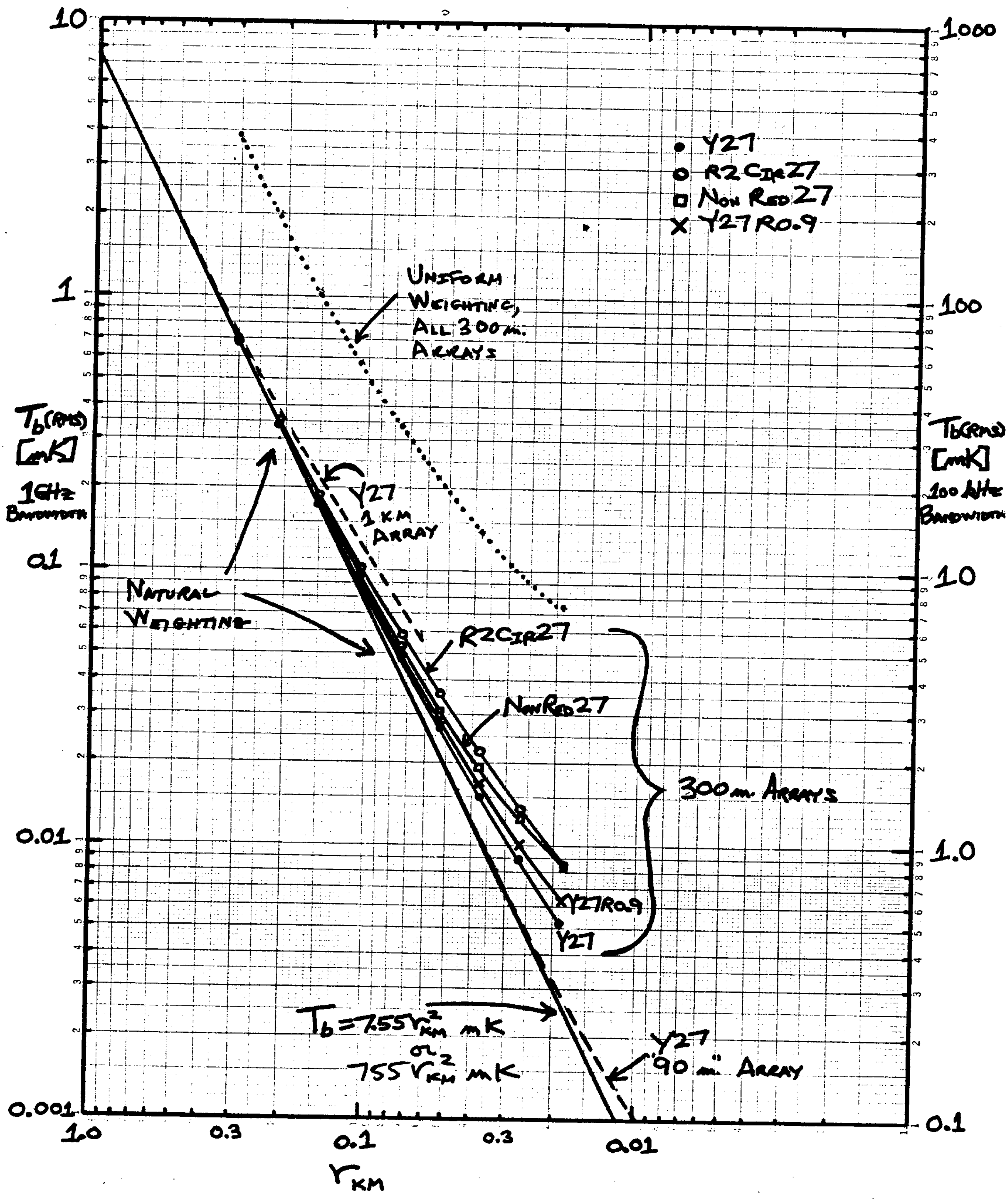

10
1
0.1
0.01
0.001
1000
100
10
1.0
0.1
Y27
R2CIR27
NON RED 27
Y27RO.9
UNIFORM WEIGHTING, ALL 300m. ARRAYS
T_b(RMS) [mK] 1GHz BANDWIDTH
Tb(RMS) [mK] 100 kHz BANDWIDTH
Y27 1 KM ARRAY
NATURAL WEIGHTING
R2CIR27
NONRED27
300m. ARRAYS
Y27RO.9
Y27
$T_b = 7.55 r_{KM}^2$ mK
or
$755 r_{KM}^2$ mK
Y27 "90 m." ARRAY
1.0
0.3
0.1
0.3
0.01
r_{KM}

Figure 15

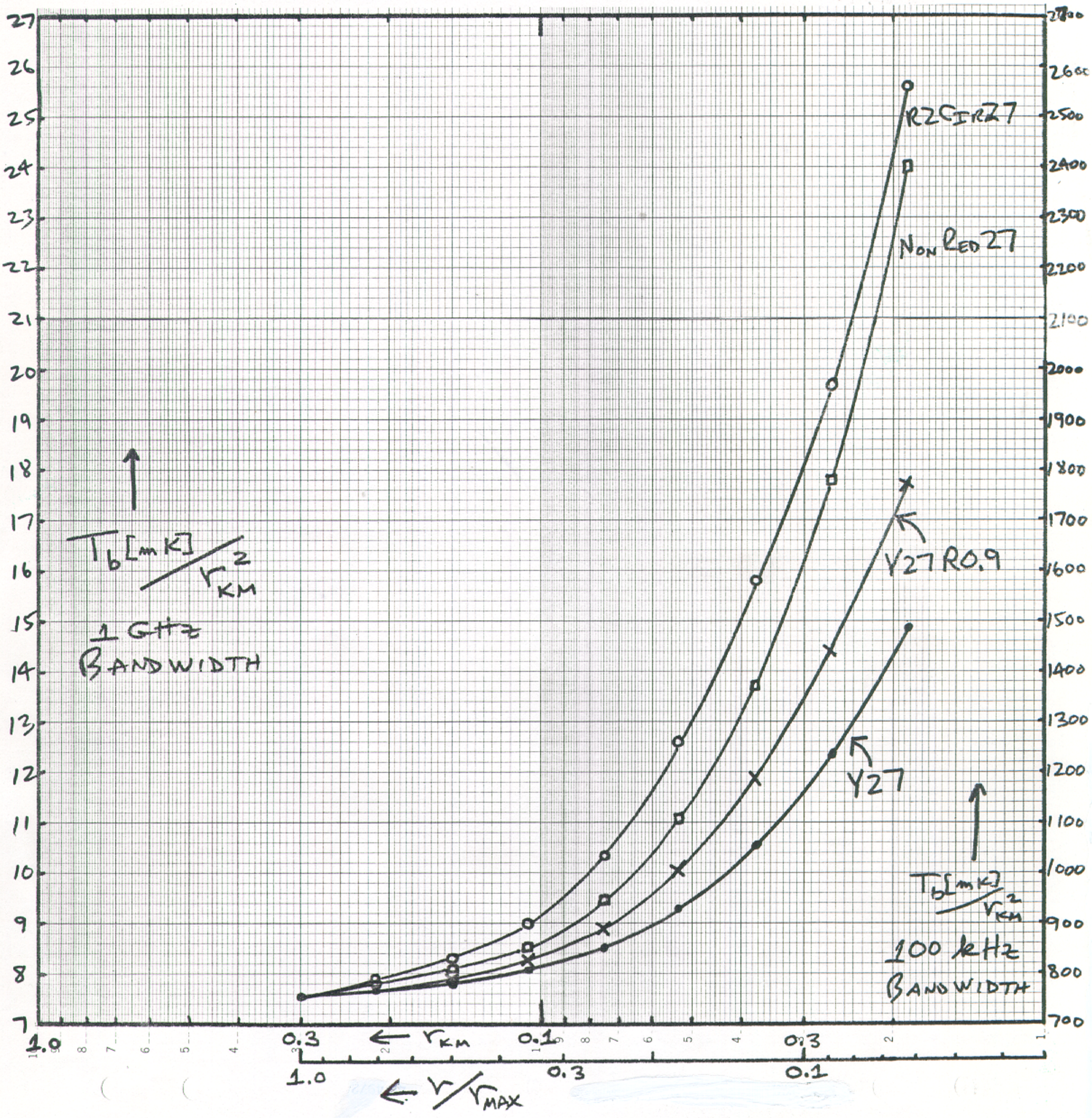

R2CIRZ27
NonRED27
Y27R0.9
Y27
Tb[mK] / r_KM^2
1 GHz BANDWIDTH
100 kHz BANDWIDTH
← r_KM
← r/r_MAX

Figure 16